Article:

Binny, Rachelle N, Law, Richard orcid.org/0000-0002-5550-3567 and Plank, Michael (2019) Living in groups: spatial-moment dynamics with neighbour-biased movements. Ecological Modelling. 108825. ISSN: 0304-3800

https://doi.org/10.1016/j.ecolmodel.2019.108825

Living in groups: spatial-moment dynamics with neighbour-biased movements

Rachelle N. Binny[1,2], Richard Law[3], Michael J. Plank[2,4,*]

1. Manaaki Whenua Landcare Research, Lincoln 7640, New Zealand.
2. Te Pūnaha Matatini, New Zealand.
3. Department of Biology, University of York, York YO10 5DD, United Kingdom.
4. School of Mathematics and Statistics, University of Canterbury, Christchurch 8140, New Zealand.

* Corresponding author email: michael.plank@canterbury.ac.nz

Abstract

Herd formation in animal populations, for example to escape a predator or coordinate feeding, is a widespread phenomenon. Understanding which interactions between individual animals are important for generating such emergent self-organisation has been a key focus of ecological and mathematical research. Here we show the relationship between the algorithmic rules of herd-forming agents, and the mathematical structure of the corresponding spatial-moment dynamics. This entails scaling up from the rules of individual, herd-generating behaviour to the macroscopic dynamics of herd structure. The model employs a mechanism for neighbour-dependent, directionally-biased movement to explore how individual interactions generate aggregation and repulsion in groups of animals. Our results show that a combination of mutually attractive and repulsive interactions with different spatial scales is sufficient to lead to the stable formation of groups with a characteristic size.

Keywords: collective behaviour; herd formation; moment closure approximation; neighbourhood interactions; spatial point process.

1 Introduction

The self-organisation of animals into herds, and the use of individual-based models to learn about the rules underlying this process, is a core subject in behavioural ecology (Krause et al., 2002). Herd formation is most often considered in terms of movements of individuals, biased by their interactions at small spatial scales. However, these movements can affect the dynamics of populations and communities at larger spatial scales. In his seminal work, "Geometry for the selfish herd", Hamilton (1971) proposed that aggregation of animals into groups or herds, could be driven by the 'selfish' desire of an animal to reduce its predation risk by manoeuvring to positions that would place other population members closer to the predator. Underlying this idea was the concept of an animal's *domain of danger*, a region of space containing all points nearer to that individual than to any other individual. The larger an animal's domain of danger, the greater its risk of predation, and Hamilton therefore theorised that aggregation arose simply due to each animal undergoing movements towards its nearest neighbour, to reduce the size of its domain of danger. Stemming from this original idea, James et al. (2004) considered a model with greater biological realism, by incorporating a *limited domain of danger*, representing either a limited detection range or attack range of predators, that could be applied to animal groups of finite size. Further work by Reluga and Viscido (2005) pointed out that rules for generating realistic selfish herds need interactions beyond an individual's nearest neighbours, and showed how predation-based selection could increase the influence of distant neighbours. Other models explored animal aggregation behaviour by introducing sensory zones of individuals, for example zones of repulsion or attraction that drive animals towards or away from neighbouring individuals, giving rise to higher order structure in the population (Couzin et al., 2002; Wood and Ackland, 2007; Bode, 2011; Herbert-Read et al., 2011). One such model, proposed by Lukeman et al. (2010), used imagery data to infer individual zones of repulsion-alignment-attraction to describe self-aggregation in surf scoter flocks.

In addition to individual-based models, other common modelling approaches for herd formation involve the use of mathematical equations of motion for individuals or populations. For example, "Lagrangian" equations of motion describe individuals' trajectories in terms of forces and velocities. "Eulerian" continuum equations (i.e. partial differential equations), based on a diffusion approximation of random motion, are also widely employed to describe the evolution (in time and space) of mean-field density for swarms (Parrish and Edelstein-Keshet, 1999). The key problem with mean-field models is that they consider only the first spatial moment (the average density of individuals) and invoke an assumption that all individuals interact in proportion to this average density (i.e. equivalent to assuming a well-mixed population or that all interactions are long-ranged), thereby ignoring any spatial structure in a population. This can give misleading results for systems where spatial structure is an important driver of the population dynamics (Law et al., 2003).

Models for the dynamics of spatial moments deal explicitly with local spatial structure, and avoid the limitations of mean-field models by using higher-order spatial moments. The second spatial moment, i.e. the density of pairs of individuals as a function of their spatial separation, carries information on local spatial structure, and there is now a substantial body of theory for spatial-moment dynamics up to second order for birth-death-movement processes (Bolker and Pacala, 1997; Dieckmann and Law, 2000; Murrell and Law, 2003). This theory has been extended to consider multiple interacting species (Plank and Law, 2015), for example in predator-prey systems (Murrell, 2005; Barraquand and Murrell, 2013). A formal mathematical derivation that allows construction of a dynamical system for the second spatial moment in the presence of directionally-biased movement has been given by (Middleton et al., 2014; Binny et al., 2015, 2016a) and extended to include birth and death processes (Binny et al., 2016b). This mechanism for neighbour-dependent directional bias has been shown to be a strong driver of spatial structure, such as aggregation, in motile cell populations (Binny, 2016). The directionally-biased movement modelling framework has been extended to multiple species by Surendran et al. (2018b) in the context of cell–obstacle interactions and by Surendran et al. (2018a) to chase–escape dynamics. However, directional movement of animals, as they respond to cues from their neighbourhoods, have not previously been part of this framework (but see Murrell and Law (2000) for nondirectional, environment-dependent movement).

Spatial moment dynamics are capable of providing mechanistic understanding of the effects of individual interactions that repeated simulations of individual-based models alone cannot. Although it is not typically possible to obtain closed-form solutions for the spatial moments, which must be approximated numerically, the structure of the equations can provide analytical insights into the relationships between model parameters and solutions. For example, spatial moment approximations have revealed: how and why spatial structure affects population carrying capacity (Law et al., 2003); new mechanisms for coexistence (Murrell and Law, 2003); the relative importance of different drivers of spatial structure (Binny et al., 2016b); and an analytical equivalence between mean population density and interaction range (Binny, 2016). Although straightforward to simulate in principle, individual-based models are stochastic processes with a very high dimensional state space and are not amenable to analytical approaches except in special cases (Blath et al., 2007). In addition, although individual-based models are relatively efficient to simulate for small populations, the computational cost for models with interactions among individuals increases faster than linearly with population size (Binny et al., 2016b). In contrast, the computational cost of solving a spatial moment dynamics approximation is insensitive to population size (Surendran et al., 2018b) so this represents an efficient alternative to individual-based models for large or growing populations.

The purpose of this paper is two-fold. First, we employ new mathematical theory recently developed in the context of collective cell behaviour, that allows scaling up from directionally-biased agent movements to macroscopic dynamics (Binny et al., 2016a; Surendran et al., 2018b), and demonstrate how it can be applied in the ecological setting of herd formation in animals. The key mathematical expressions encoded in the rules of the individual-based model become clear in doing this. Secondly, we show that the spatial properties of herd formation are captured by the macroscopic dynamics, through appropriate choice of interaction kernels for directionally-biased movement. **This provides a foundation to bring biased movement into the earlier models of spatial-moment dynamics that focus on births, deaths and unbiased movement (Plank and Law, 2015). The framework will enable herd development to be studied in the broader context of population and community dynamics. To facilitate this future work, the mathematical derivations are given in a multi-species setting.**

2 Stochastic, individual-based model

Spatial-moment dynamics of birth, death and growth processes have been dealt with previously (Bolker and Pacala, 1997; Dieckmann and Law, 2000; Murrell and Law, 2003; Adams et al., 2013). Therefore here we consider only movement of individuals of fixed types. We first consider an individual-based model for motile agents. For generality, we allow individuals to be of an arbitrary number of types, indexed $i \in \{1, ..., i_{\max}\}$. These could be species allowing, for instance, spatial interactions of predators and herd-living prey (the indexing can be ignored if all individuals are of the same type). Processes take place in a continuous two-dimensional space, which is large compared with the scale over which individuals interact and move; a point in the space is given by the vector $x = (x_1, x_2)$ of Cartesian coordinates.

2.1 Model for biased movement

The population comprises a fixed number n of individuals numbered $p = 1, \ldots, n$, and the state at time t is characterised by their types and locations (i_p, x_p). Individual p moves in a series of discrete steps, which occur at a rate M_p that may depend on its neighbourhood. This is a Poisson process over time, so the probability of movement in a short period δt is $M_p \delta t + O(\delta t^2)$. Movement events are assumed to occur as instantaneous jumps (i.e. a position jump process). As soon as a movement takes place, the state of the system is changed, potentially leading to a change in M_p as well.

We allow both an intrinsic and a neighbourhood contribution to the movement rate, given by

$$M_p = m_{i_p} + \sum_{q \neq p} w_{i_p i_q}(x_p, x_q). \tag{1}$$

Here m_i is the intrinsic component of the movement rate for type i, and $w_{i_p i_q}(x_p, x_q)$ is an extra contribution to the movement rate caused by a neighbouring individual q of type i_q at location x_q. The contribution may depend on the location and type of both p and q. The weight typically attenuates with distance from p to q and could depend on whether individual q is the same species or, say, a predator species. The overall effect of neighbours is obtained by summing over all q, excluding individual p itself.

When individual p moves from x_p, it jumps to another location $u_p = x_p + \xi$ where ξ is a random variable in $\mathbb{R}^2$ with a bivariate probability density function (PDF) of the form

$$\hat{\mu}_p(\xi) = f_{i_p}(|\xi|)\hat{g}_p\left(\arg(\xi)\right), \tag{2}$$

where $\arg(\xi) \in [0, 2\pi)$ denotes the direction of the vector ξ. The PDF in Eq. (2) is separated into two independent parts for the distance moved $|\xi|$ and the direction of movement $\arg(\xi)$. For simplicity, we assume that $f_i(|\xi|)$ is neighbourhood-independent (though it may depend on the individual's type i) and given by the Gaussian function with mode r_i and variance s_i^2:

$$f_i(|\xi|) = C_i e^{-\frac{(|\xi| - r_i)^2}{2s_i^2}}, \qquad 0 \leq |\xi| \leq r_{i,\max}, \tag{3}$$

where C_i is a normalisation constant. In contrast to the distance moved, the direction of movement does depend on the neighbourhood of individual p, and is the core mechanism underpinning herd development here. The neighbourhood dependence takes the form of a bias vector $\hat{\eta}_p$ for individual p, defined below, that provides the parameters for a circular probability distribution for the direction of movement.

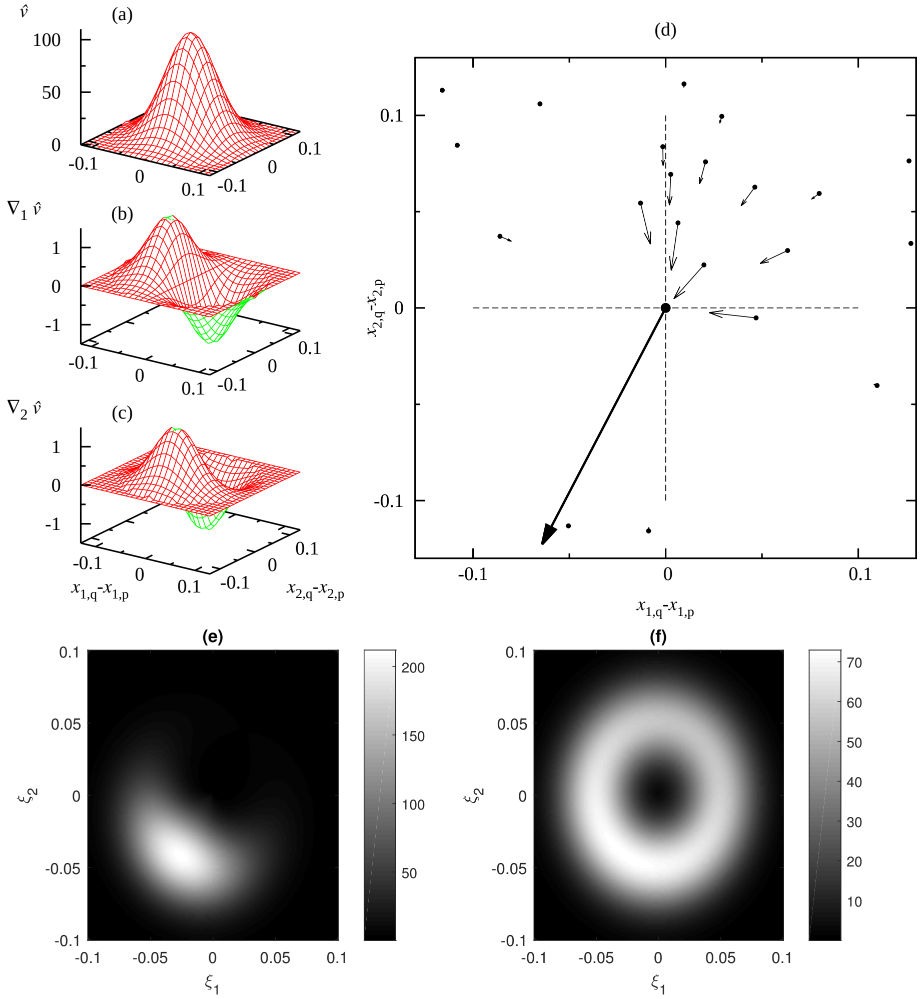

Figure 1: Schematic diagram showing how the bias vector and the movement distribution of a focal individual are constructed. (a) A bias kernel v, from which the gradient vector ∇v, whose x_1, x_2 components are plotted in (b) and (c), is obtained. (d) Contribution of neighbouring individuals (light arrows) to the bias vector of the focal individual at the origin (bold arrow). Note that the light arrows are not the bias experienced by the neighbouring individuals, but their contribution to the bias of the focal individual. The direction of the bias vector determines the preferred direction and its magnitude determines how tightly peaked the distribution is around the preferred distribution. Note the bias vector does not determine the new location of the focal individual. (e, f) Bivariate probability density function Eq. (2) for the movement vector ξ of the focal individual in the case of strong bias ($\beta = 0.15$) and weak bias ($\beta = 0.01$) respectively. Movement distance is distributed according to Eq. (3) with $r = 0.05$, $s = 0.02$, $r_{\max} = r + 3s$.

The bias vector is obtained from the gradient vector of a bias kernel function that carries the key biological information. As an example, we describe the construction of a bias vector for a single focal individual located at the origin in Fig. 1. This starts with a bias kernel function $v_{i_p i_q}(x_q - x_p)$, here a standard Gaussian function of the distance $x_q - x_p$ between two individuals (Fig. 1a), potentially dependent on both the focal individual's type i_p and the neighbouring individual's type i_q. The kernel gives a gradient vector $\nabla v_{i_p i_q}(x_q - x_p)$, i.e. the partial derivatives of $v_{i_p i_q}$ in the two spatial dimensions (Fig. 1b, c). The contribution of neighbouring individual q of type i_q and location x_q to the bias vector of the focal individual p is the gradient vector evaluated at $x_q - x_p$ (light arrows on neighbouring individuals in Fig. 1d). A neighbour vector that points towards the origin corresponds to a repulsive effect of the neighbour on the focal individual (an outward arrow would be an attractive effect). Summing all neighbour vectors gives the bias vector for the focal individual (bold arrow on the focal individual in Fig. 1d):

$$\hat{\eta}_p = \beta_{i_p} \sum_{q \neq p} \nabla v_{i_p i_q}(x_q - x_p), \tag{4}$$

where β_{i_p} is a parameter scaling the overall strength of bias. In the example (Fig. 1d), the neighbourhood gives the focal individual a preferred direction of movement away from the cluster of individuals on its upper right-hand side. Note that changing the sign of the bias kernel in Fig. 1a would reverse the direction of all arrows in Fig. 1d and hence produce an attractive rather than a repulsive bias.

Once the bias vector $\hat{\eta}_p$ for individual p is computed, its direction of movement θ is drawn from the von Mises distribution (independent of the distance moved) with preferred direction $\arg(\hat{\eta}_p)$ and concentration $|\hat{\eta}_p|$. This distribution has probability density function

$$\hat{g}_p(\theta) = g(\theta, \hat{\eta}_p) = \frac{\exp\left(|\hat{\eta}_p| \cos\left(\theta - \arg(\hat{\eta}_p)\right)\right)}{2\pi I_0\left(|\hat{\eta}_p|\right)}, \tag{5}$$

where I_0 is the modified Bessel function of the first kind and zero order. If the magnitude of the bias vector is large, the von Mises distribution is tightly peaked around $\arg(\hat{\eta}_p)$, meaning the individual is highly likely to move in a direction close to the preferred direction (Fig. 1e). This situation would arise if the focal individual has multiple near neighbours exerting bias in similar directions (as in the example in Fig. 1d). Conversely, if the magnitude of the bias vector is small, the von Mises distribution is more broadly distributed (Fig. 1f). In the limit where the bias vector has zero magnitude, the von Mises distribution is a uniform distribution on $[0, 2\pi)$, meaning the focal individual is equally likely to move in any direction. This situation would arise if the focal individual has no near neighbours, or has neighbours that are symmetrically positioned on opposite sides such that their contributions to the bias vector cancel one another out.

2.2 Implementation

We initialised realizations of the stochastic individual-based process with a fixed population of $n = 200$ individuals of a single type. The individuals were distributed in a unit arena as a spatial Poisson process at the start of each realization; in other words, each individual's location was chosen uniformly at random and independently of all other individuals. Distances are given relative to the unit of the arena. We used periodic boundary conditions, and updated the state of the system in continuous time using the Gillespie algorithm (Gillespie, 1977). For simplicity, we assumed the movement rate to be independent of neighbourhood by setting $w_{i_p i_q} = 0$ for all p and q in Eq. (1), leaving in place only an effect of neighbours on the direction of intrinsic movements.

Eqs. (2)–(5) define the bivariate movement distribution of a focal individual p. Vectors ξ from this bivariate distribution were obtained by independently generating the distance and direction of movement. The probability that the distance moved $|\xi|$ by an individual of type i lies in the infinitesimal interval $[r, r + dr]$ is $r f_i(r)\, dr$. Hence, movement distance of an individual of type i has PDF

$$h_i(r) = r f_i(r).$$

Random numbers from this distribution were generated via the following rejection sampling algorithm:

1. Generate a normally distributed random number $R \sim N(r_i, s_i^2)$
2. If R lies outside the interval $[0, r_{i,\max}]$, go to step 1. This results in a sample from the distribution with PDF $f_i(r)$ specified by Eq. (3).
3. Accept R with probability $P(R) = R/r_{i,\max}$, otherwise go to step 1. This results in a sample from the distribution with PDF $h_i(r)$ as required.

The direction of movement θ was generated from the von Mises distribution with PDF given by Eq. (5). This requires the bias vector $\hat{\eta}_p$ for individual p to be calculated, according to Eq. (4).

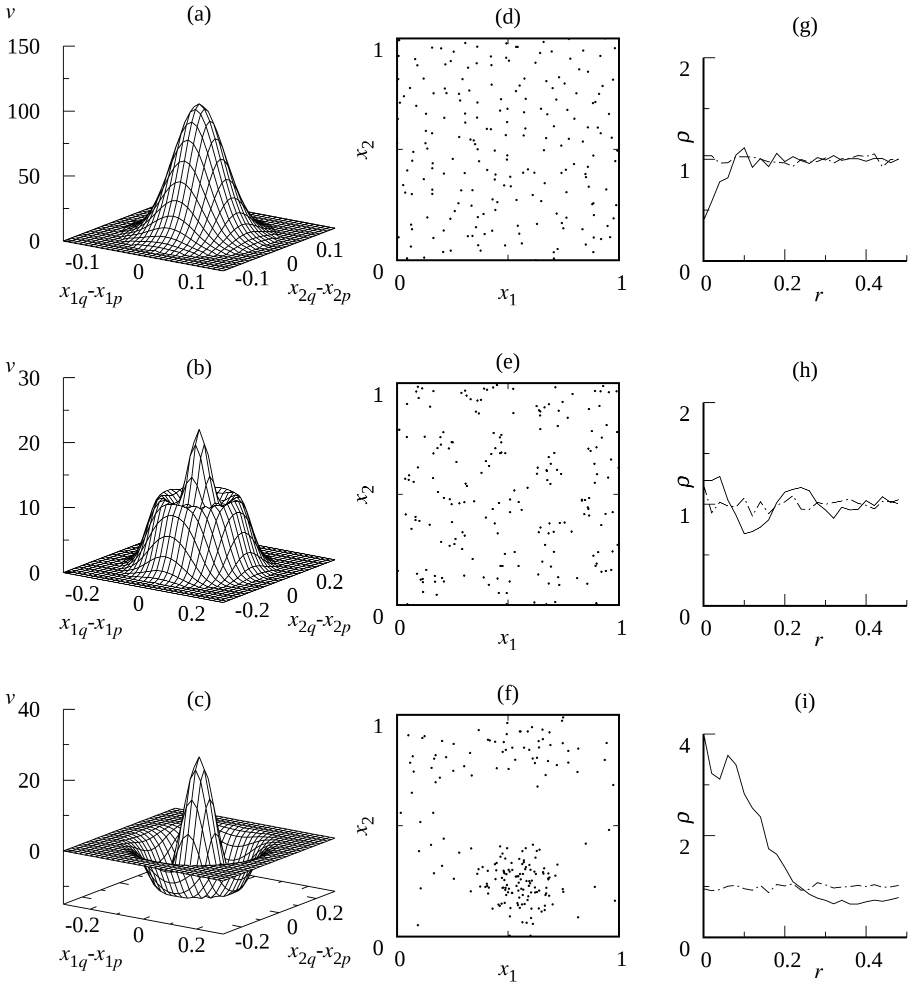

Figure 2: Territories and clusters developing from contrasting bias kernels. (a) A single positive Gaussian function Eq. (6) ($\sigma_1 = 0.04$, $N = 0.0099$) leads to formation of territories. (b) Adding a second Gaussian function, Eq. (7), that peaks at a distance $\bar{r} = 0.12$ from the origin ($\sigma_1 = \sigma_2 = 0.04$, $N = 0.0477$, $k_2 = 0.5$) leads to small clusters. (c) Subtracting a second Gaussian function, Eq. (7), that reaches its minimum at a distance $\bar{r} = 0.12$ from the origin ($\sigma_1 = \sigma_2 = 0.04$, $N = 0.0401$, $k_2 = -0.5$) leads to a single large cluster. Gaussian functions in the bias kernels were truncated at ± 3 standard deviations. Bias strength of the gradient vector $\beta = 0.01$. (d),(e),(f) Snapshots of locations of individuals at time $t = 10$; the spatial patterns change continuously over time, starting from a spatial Poisson process. (g),(h),(i) Contrasting pair correlation functions $\rho(r)$ of the spatial patterns develop by $t = 10$ (continuous lines, $\delta r = 0.02$); the dash-dot lines show $\rho(r)$ at time $t = 0$. Neighbourhoods act only on the direction of movement here, not on the rate of movement. Movement distance is distributed according to Eq. (3) with $r = 0.05$, $s = 0.02$, $r_{\max} = r + 3s$. Movement rate $m = 1$.

2.3 Biased-movement kernels and spatial structure

The choice of a kernel for biased movement is a biological matter with far-reaching consequences. Fig. 2 gives three examples. The first is a single Gaussian function centred on the origin

$$\text{(a): } v_{i_p i_q}(r) = \frac{1}{N} e^{-r^2/2\sigma_1^2} \tag{6}$$

where $r = |x_q - x_p|$ is the distance of neighbour q from focal individual p, σ_1 is a measure of the width of the function, and N is a normalisation constant. The second and third examples combine a Gaussian function centred on the origin with one offset from the origin by an amount $\bar{r}$ and with width σ_2:

$$v_{i_p i_q}(r) = \frac{1}{N} \left(e^{-r^2/2\sigma_1^2} + k_2 e^{-(r-\bar{r})^2/2\sigma_2^2} \right) \tag{7}$$

the weight k_2 of the outer function having different signs: (b) $k_2 > 0$, and (c) $k_2 < 0$.

A kernel based on the single Gaussian function generates a gradient vector that points towards the origin, creating a region of repulsion around each individual. This means that individuals tend to move away from near neighbours (Fig. 2a), leading to territory formation (Fig. 2d). A kernel based on a double Gaussian function in which the outer Gaussian is positive ($k_2 > 0$, Fig. 2b), generates three concentric rings: an inner ring where the gradient vector points towards the origin, an intermediate ring where it points away from the origin, and an outer ring where it points towards the origin. This creates short-range repulsion, medium-range attraction and long-range repulsion, leading individuals to form small clusters (Fig. 2e). A kernel based on a double Gaussian function, in which the outer Gaussian is negative ($k_2 < 0$, Fig. 2c), generates two concentric rings: an inner ring where the gradient vector points towards the origin, and an outer ring where it points away from the origin. This creates short-range repulsion and long-range attraction, leading towards coalescence of the population into a single mega-herd (Fig. 2f). The reverse order (attraction-repulsion) would lead to collapse of individuals within groups to a single point, which would not be not biologically reasonable.

Short-range repulsion (Fig. 2a, d) creates space around indviduals, and is a natural basis for territories, defended by individuals or groups, that come about from scarcity of resources (Maher and Lott, 1995). Adding longer-range attraction (Fig. 2c, f) allows for benefits of living in groups, such as a reduced risk of predation, increased chance of detecting predators, and less need for individual vigilance (Hamilton, 1971; Pulliam, 1973; Elgar, 1989). With the short-range repulsion still in place, some space around individuals remains and this can lead to remarkable spatial structure, such as that observed in king penguin colonies (Gerum et al., 2018). However, the combination of local repulsion and longer-range attraction can lead to very large groups forming (Olson et al., 2009). In practice, populations often break up into much smaller groups because of the costs of living together, such as the need for synchronized behaviour (Gajamannage et al., 2017), levels of stress (Markham et al., 2015), possibly the spread of disease (Griffin and Nunn, 2012; Sah et al., 2017), and competition/cooperation between males (DuVal, 2007). Adding a further outer region of repulsion (Fig. 2b, e) allows break-ups to happen, the smaller groups being distributed non-randomly over space, with spatial structure inside the groups themselves.

The spatial structures in Fig. 2 are clearly quite different, and this difference is summarised in their pair correlation functions (Fig. 2g,h,i). A pair correlation function $\rho_{ij}(r)$ is a standard, second-order spatial statistic, based on the density of pairs of points of type i, j as a function of the distance r between them (Illian et al., 2008). In the absence of spatial structure at a distance r, $\rho_{ij}(r)$ takes a value 1; if there is an excess of pairs (clustering), $\rho_{ij}(r) > 1$; if there is a lack of pairs (regular pattern), $\rho_{ij}(r) < 1$. Thus the space that individuals create around themselves in Fig. 2d shows up as a lack of pairs at short distance in the pair correlation in Fig. 2g. The clusters that form in Fig. 2e appear as an excess of pairs at short distances in Fig. 2h, and a lack of pairs at slightly longer distances. The clusters themselves are not distributed at random across space, and leave an attenuating oscillatory signal in the pair correlation as distance increases. The location of the secondary peak in Fig. 2h at around $r = 0.2$ corresponds to the typical distance between adjacent clusters. The mega-herd developing in Fig. 2f appears as a large peak of pairs at short distances from the interaction of local repulsion and longer-distance attraction, with pairs becoming less frequent beyond the peak (Fig. 2i). The function does not tend to 1 at large distances, because the cluster is on the same spatial scale as the arena.

At a single point in time, repeated realizations of the stochastic processes from the same initial statistical distribution have different spatial configurations, but the same basic information is retained in the pair correlation functions. As time goes on, the spatial patterns change, and the pair correlation functions track the developing spatial structure. This tracking is evident in Fig. 2g,h,i. The realizations all started as Poisson processes lacking spatial structure, and with pair correlation functions close to 1 at all distances. But, by $t = 10$, the functions are quite distinct from one another, as shown in Fig. 2. The significance of the time-dependent pair correlation becomes important below, because a measure of this kind becomes the state variable of the spatial-moment dynamics. In some ecological systems, statistical stationarity may eventually be reached. But in others, such as predator-prey systems, it is conceivable that the pair correlation functions could develop periodic behaviour and continue to change indefinitely. The long-term behaviour of the pair correlation function under a given choice of bias kernel is not sensitive to the particular choice of initial conditions.

3 Spatial-moment dynamics

Here we show how the algorithmic rules of the individual-based stochastic process can be described mathematically to give deterministic approximation in the form of a dynamical system for the second spatial moment.

3.1 Definition of spatial moments

In defining the spatial moments, it helps to think of small regions of area h, so that the $O(h^2)$ probability of containing more than one individual is vanishingly small. Formally, the first spatial moment at time t is the expected value of the density obtained from the stochastic process at time t, in the limit as $h \to 0$:

$$Z_{1,i}(x) = \lim_{h \to 0} \frac{E[n_i(\delta x)]}{h}, \tag{8}$$

where $n_i(\delta x)$ is the number of individuals of type i in the region δx centred on x.

In the case of the second moment, we consider two regions of area h: δx centred on x containing n_i individuals of type i, and δy centred on y containing n_j individuals of type j. The second spatial moment at time t is the expected value of the pair density from the stochastic process at time t, in the limit as $h \to 0$ (Plank and Law, 2015):

$$Z_{2,ij}(x, y) = \lim_{h \to 0} \frac{E[n_i(\delta x) n_j(\delta y) - \delta_{ij} n_i(\delta x \cap \delta y)]}{h^2}. \tag{9}$$

The second term in the numerator (with Kronecker delta δ_{ij}) is needed to remove a pair that i in δx would otherwise create with itself. Below we also use the third moment, the density of triplets $Z_{3,ijk}(x, y, z)$, defined in a similar way after removing all non-distinct triplets (Plank and Law, 2015).

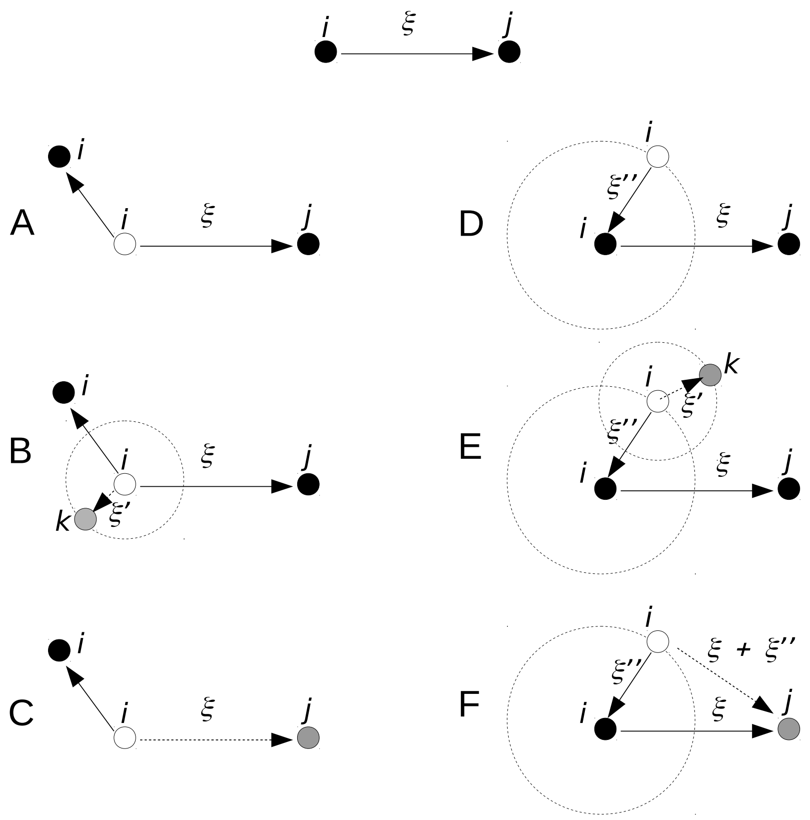

Figure 3: Geometry of the six flux terms A, ..., F in which movement of an individual of type i changes the pair density $Z_{2,ij}(\xi)$ in a model of spatial-moment dynamics, numbered as described in the text. The object at the top is the ij pair: an individual of type j displaced by ξ from the focal individual of type i. Black-filled circles are locations of individuals after movement; empty circles are the positions from which they move; grey circles are neighbours that affect the movement; a dotted circle represents an integration over a neighbourhood; arrows are vectors. Geometries A, B, C in the first column destroy the pair; geometries D, E, F in the second column create the pair. A, ..., F are given as formal expressions (10), ..., (15) in the text.

3.2 Dynamics of the second moment

For simplicity, we consider dynamics in a homogeneous space, meaning that the statistics of the spatial point process in any subdomain are the same, regardless of the location of that subdomain. In this case, the first spatial moment $Z_{1,i}$ is independent of spatial location x. Further, since the model consists only of movement and there is no birth or death, there is no change in first moment over time, so the first moment is simply a constant determined by the fixed population size. The second spatial moment $Z_{2,ij}$ can be expressed as a function of the displacement vector between two individuals $\xi = y - x$, rather than as a function of their physical locations x and y (see Fig. 3 for geometric interpretation). Similarly, the third moment $Z_{3,ijk}$ can be expressed in terms of two displacement vectors, $\xi = y - x$ and $\xi' = z - x$.

Although the first moment is constant, the second moment does change over time as spatial structure develops, as was evident from the pair correlation functions in Fig. 2. The second moment and all higher moments are functions of time, but for clarity we omit the time argument below. The normalised second moment $Z_{2,ij}(\xi)/(Z_{1,i}Z_{1,j})$ relates to the measure of spatial structure in Fig. 2g,h,i; it is the expected value of the pair correlation function $\rho_{ij}(r)$ under isotropy. Thus, to follow the dynamics of the second moment is equivalent to following the behaviour of the average pair correlation function over time. In other words, the dynamics track the development of spatial structure over time. With $Z_{2,ij}(\xi)$ as the state variable, we have a dynamical system describing changes in a function, as opposed to a dynamical system of a scalar quantity, the density of individuals (i.e. we have a partial as opposed to an ordinary differential equation). This is to be expected because the dynamical system has to carry information about the location of individuals relative to one another.

A formal derivation from the stochastic process (Binny et al., 2015, 2016a) leads to six terms affecting the rate of change in the second moment $Z_{2,ij}(\xi)$ due to movement by the focal individual of type i, labelled (A)–(F) below and with geometries illustrated in Fig. 3. Symmetric terms corresponding to movement of the other individual (of type j) in the pair are obtained by making the transformation $\langle i, j, \xi \to j, i, -\xi \rangle$ to each of the terms below.

First are three negative terms that account for the ways in which an existing pair, consisting of a individual of type i separated from an individual of type j by a vector ξ, can be destroyed. Bias in the movement direction does not enter into these terms, because movement by the focal individual in any direction destroys the pair.

(A) Intrinsic rate of movement m_i of the focal individual:

$$f_A = -Z_{2,ij}(\xi)m_i. \tag{10}$$

(B) Effect of the neighbourhood of the focal individual on its movement rate:

$$f_B = -\sum_k \int Z_{3,ijk}(\xi, \xi')w_{ik}(\xi')d\xi'. \tag{11}$$

This incorporates the density of neighbours of type k displaced by ξ' from the focal individual (conditional on the presence of the individual of type j displaced by ξ from the focal individual), given by the third moment $Z_{3,ijk}(\xi, \xi')$. The kernel function $w_{ik}(\xi')$ gives a weight to the effect of the neighbour on the movement rate of the focal individual. The overall effect of the neighbourhood is then obtained by integrating over all displacements ξ' and summing over all types k.

(C) The other individual (of type j) in the pair also affects the movement rate of the focal individual, with a contribution weighted by $w_{ij}(\xi)$:

$$f_C = -Z_{2,ij}(\xi)w_{ij}(\xi). \tag{12}$$

Mirroring the negative terms are three positive terms that account for the ways in which a pair, consisting of an individual of type i separated from an individual of type j by a vector ξ, can be created. Since this can only occur via movement, this always starts with an ij pair separated by a different vector, denoted $\xi + \xi''$, followed by a movement by vector ξ''. These terms are more intricate than those in Eqs. (10)–(12) because they have to cover all possible starting locations for the focal individual and this needs to allow for bias in movement direction.

(D) Intrinsic movement rate of the focal individual, allowing for all starting points:

$$f_D = m_i \int Z_{2,ij}(\xi + \xi'')\mu_{ij}(\xi'', \xi + \xi'')d\xi''. \tag{13}$$

Here, the term inside the integral is the probability of starting with an ij pair separated by vector $\xi + \xi''$, followed by a movement by ξ'' of the individual of type i, which happens with probability density $\mu_{ij}(\xi'', \xi + \xi'')$ (see below). This is then integrated over ξ'' to allow for all possible starting locations.

(E) Effect of the neighbourhood of the focal individual on its movement rate, depending on its starting location:

$$f_E = \int \mu_{ij}(\xi'', \xi + \xi'')\left(\sum_k \int Z_{3,ijk}(\xi + \xi'', \xi')w_{ik}(\xi')d\xi'\right)d\xi''. \tag{14}$$

This is similar in structure to (11), accounting for the influence on the focal individual's movement rate of a third individual of type k at displacement

ξ''. The outer integral over ξ'' allows for all possible starting locations for the focal individual.

(F) The other individual (of type j) in the pair also affects the movement rate of the focal individual:

$$f_F = \int Z_{2,ij}(\xi + \xi'')\mu_{ij}(\xi'', \xi + \xi'')w_{ij}(\xi + \xi'')d\xi''. \tag{15}$$

This is similar in structure to (13), but instead of the intrinsic movement rate m_i, accounts for the contribution to the focal individual's movement rate from the other individual (of type j) in the pair. When the pair is initially separated by vector $\xi + \xi''$, this contribution is $w_{ij}(\xi + \xi'')$. Again, the integral over ξ'' allows for all possible starting locations.

The key ecological information for movement bias is contained in $\mu_{ij}(\xi'', \xi + \xi'')$, which is the probability density that the focal individual's movement vector is ξ'', conditional on the presence of an individual of type j located at $\xi + \xi''$ relative to the focal individual. This is the movement vector needed to create the ij pair separated by ξ as required. As with the stochastic model (Eq. (2)), this is composed of two independent parts:

$$\mu_{ij}(\xi'', \xi + \xi'') = f_i(|\xi''|)g(\arg(\xi''), \eta_{ij}(\xi + \xi'')). \tag{16}$$

The first part $f_i(|\xi''|)$ relates to the distance moved by an individual of type i, which is independent of the neighbourhood and given by Eq. (3). The second part $g(\arg(\xi''), \eta_{ij}(\xi + \xi''))$ is the probability density of moving in direction $\arg(\xi'')$, which does depend on the neighbourhood. This dependence is encapsulated in the expected bias vector $\eta_{ij}(\xi + \xi'')$ for an individual of type i separated from an individual of type j by a vector $\xi + \xi''$:

$$\eta_{ij}(\xi + \xi'') = \beta_i \left(\sum_k \int \nabla v_{ik}(\xi') \frac{Z_{3,ijk}(\xi + \xi'', \xi')}{Z_{2,ij}(\xi + \xi'')} d\xi' + \nabla v_{ij}(\xi + \xi'') \right) \tag{17}$$

Here $\nabla v_{ik}(\xi')$ is the gradient vector of the bias kernel $v_{ik}(\xi')$. Eq. (17) integrates over the neighbourhood of the focal individual for neighbouring individuals of type k, then sums over all types k, and adds the effect of the partner individual of type j in the pair. The parameter β_i gives an overall weight for the bias. The bias vector provides the parameters for a circular probability distribution. To match the stochastic model, we use a von Mises distribution with peak angle $\arg(\eta_{ij})$ and concentration $|\eta_{ij}|$, to obtain the probability density function of the angle $\arg(\xi'')$.

Summing expressions (10)–(15), gives the total rate of change of the pair density $Z_{2,ij}(\xi)$:

$$\frac{\partial}{\partial t} Z_{2,ij}(\xi, t) = f_A(\xi, t) + \cdots + f_F(\xi, t) + \langle i, j, \xi \to j, i, -\xi \rangle, \tag{18}$$

where the matching symmetric terms for the partner individual in the ij pair are given by the substitutions $\langle i, j, \xi \to j, i, -\xi\rangle$ (Plank and Law, 2015). We give the function arguments in full to make clear the time dependence. This is a formal, exact description of how the movement rules at the level of the individual translate into a dynamical system of pair densities at the macroscopic level, after averaging over many realizations of the stochastic process, starting from the same statistical distribution.

3.3 Closure of the second-moment dynamics

The dynamical system is not yet closed, because it contains the third spatial moment, the density of triplets. To deal with this, a closure approximation is needed to replace the third moment by a function of lower-order moments. Although not usually recognized, closures are ubiquitous in ecological theory: ignoring spatial structure completely implies a closure of the form $Z_{2,ij}(\xi) = Z_{1,i}Z_{1,j}$, giving a dynamical system for the first moment (average density), i.e. the law of mass action, or the so-called mean-field assumption. A formal theory of closures at second order is a matter for research (Raghib et al., 2011; Dieckmann and Law, 2000; Murrell et al., 2004). Here, we use the Kirkwood closure (Kirkwood, 1935):

$$Z_{3,ijk}(\xi, \xi') = \frac{Z_{2,ij}(\xi)Z_{2,ik}(\xi')Z_{2,jk}(\xi' - \xi)}{Z_{1,i}Z_{1,j}Z_{1,k}} \tag{19}$$

as we have found the exact choice of closure makes little difference when the dynamics deal only with movement (i.e. without birth and death) (see for example Fig 6.3 in Binny (2016)).

3.4 Spatial-moment dynamics as an approximation scheme

After closure, the dynamical system is no more than an approximation for the expected value of the second moment of the stochastic process, because it ignores spatial information carried by higher-order moments. How well does this approximation work? This is analogous to asking how well the mean-field assumption works as a description of population dynamics; the answer to that question is that the approximation is poor if neighbourhoods are important (Raghib et al., 2011). The second-order closure should be better because it does carry spatial information, but would still be expected to become poor as higher-order spatial structure becomes important.

Fig. 4 compares the spatial signal of the spatial-moment dynamics with that of the stochastic individual-based model from which the dynamical

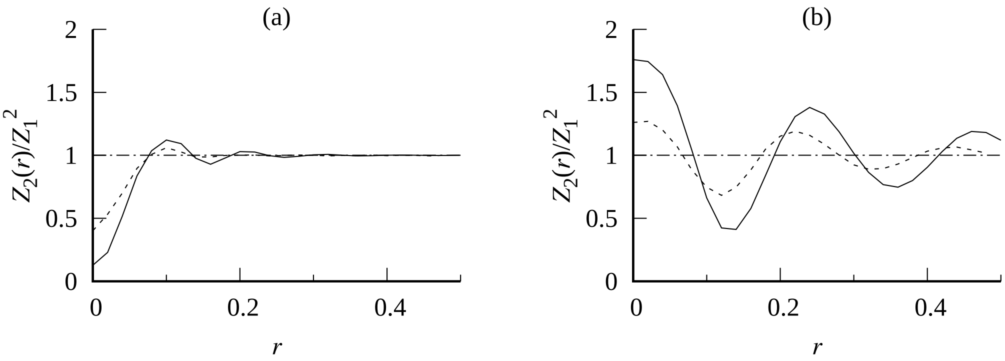

Figure 4: Solutions for the normalised pair density $Z_2(r)/Z_1^2$ of the spatial-moment dynamics, Eqs (18) (19), at time 10 (continuous lines), as a function of the distance r between the pair. These are approximations for the stochastic process of individual movement in Section 2, using parameter values that generated (a) territories in Fig. 2a, and (b) small clusters in Fig. 2b. For comparison, we also show the pair correlation functions (*sensu* Fig. 2g,h) averaged over 100 realizations of the stochastic process at time 10 (dashed lines). Initial conditions were spatial Poisson processes (dash-dot lines). Numerical integration was done by the Euler method, using Eq. (18) (19), discretised as $d\xi = 0.02, dt = 0.05$.

system (18), (19) was derived. For comparability with the stochastic results, we assumed the movement rate to be independent of neighbourhood by setting $w_{ij}(.) = 0$ in Eqs (10)–(15), and leaving in place only an effect of neighbours on the direction of intrinsic movements. This means that the spatial-moment dynamics deal only with terms (10), (13) (geometries A and D in Fig. 3). We examined the dynamics for the bias kernels shown in Fig. 2a,b, as these generate structure at a small spatial scale. We would not expect to find a good approximation with the bias kernel in Fig. 2c, because spatial structure remains at large spatial scales. In other words, the pair correlation $\rho(r)$ does not approach 1 as r increases in Fig. 2i.

Fig. 4 shows that the approximation scheme captures some basic signals of the stochastic, individual-based model. Fig.4 shows the characteristic regular structure arising from repulsive bias, manifested as a lack of pairs at short distance. Fig. 4 shows the distinct cluster formation as a result of short-range repulsion, medium-range attraction, and long-range repulsion. Although the quantitative match between the stochastic results and the spatial moments approximation is far from perfect, the key qualitative features of the emergent spatial structure are captured in the second moment. This illustrates two key points. First, it shows that the rules responsible for generating the spatial structure in the stochastic model are encapsulated by the dynamical system of spatial moments, despite the latter appearing to be be completely different. Second it demonstrates that much of the information about spatial structure is carried just in the second spatial moment. In other words, there is some justification for closing the hierarchy at second order. The information shown in Fig. 4 would be lost completely in a mean-field model, which implicitly closes the system at the level of the first moment.

4 Discussion

This work draws on recent advances in spatial moment dynamics models of collective cell behaviour (Binny et al., 2016a; Surendran et al., 2018b) to address the issue of animal herding behaviour in ecology, and opens new research avenues in this setting. In particular, we have explored how using different forms of neighbourhood interaction kernels for directionally biased movement can give rise to formation of animal groups or herds. Individual-based models describing biased directional movement have been widely used in an ecological context (Codling and Hill, 2005; Benhamou, 2006; Codling et al., 2007; Bode, 2011). However, this is the first time that a spatial moment dynamics model, capturing the outcomes of this directional bias at the macroscopic scale, has been used to describe animals living in groups. In doing this, we have shown the geometry of six flux terms that describe the exact relationship between the algorithmic individual-based model and the mathematical model (up to the second spatial moment).

Our results show that herd-like spatial structure can be generated solely from interactions among neighbouring individuals of the same species. In reality, this spatial structure can be strongly affected by interspecific interactions, such as the presence of predators. Future work will include explicitly applying the model framework developed here to systems with multiple interacting species. This has been done for cell–obstacle interactions (Surendran et al., 2018b) and chase–escape interactions (Surendran et al., 2018a), but these models use simple attractive or repulsive interactions, rather than the distance-dependent interactions that we employ here.

One advantage of spatial moment approximations over individual-based models is that the equations for the dynamics of spatial moments are deterministic and only need to be solved once, rather than performing computationally intensive repeated simulations. They are also more tractable mathematically, permitting further analysis and exploration of parameter space. Computational power typically restricts simulation of individual-based models to systems with relatively low numbers of individuals, due to the requirements of tracking each individual's movements and interactions with each of its neighbours over time. There are many such examples of small-herd systems in ecology (see for example Table 1 in Reiczigel et al. (2008)). In contrast, the computational requirement for solving the spatial moments approximation is independent of population size. The methodology would lend itself to systems with much larger animal herds and offer insights that would otherwise require considerably greater computational resources to achieve through simulations alone.

Although the spatial-moment model shows the basic spatial structure, its fit to the stochastic model could clearly be improved. Attenuation of the spatial signal with increasing distance is rather slow in Fig 4b, which generates inaccuracies that can propagate to shorter distances. Also, at the shortest distances, the model overestimates the strength of spatial structure; this may be because, after discretisation, spatial resolution becomes less good as $r \to 0$. Such issues could be dealt with by discretising over a larger space on a finer spatial grid, but this would have made computation unfeasible. In future work, a Fourier transform for the convolution integrals should be considered, as this could provide a major increase in speed of computation.

Previous models for animals living in herds have used the idea of zones of attraction and repulsion (Couzin et al., 2002; Bode, 2011). A zone of repulsion is also supported by data (Krause et al., 2002). Zones of repulsion and attraction have also been modelled in the cell behaviour literature, for example using the Lennard-Jones kernel (Jeon et al., 2010) and the Morse potential (Middleton et al., 2014; Matsiaka et al., 2017). Our model incorporates and builds on these ideas, including the possibility for multiple zones of attraction and repulsion with different spatial scales. Examples of the types of behaviour encapsulated by the bias kernels we have studied, and the resulting spatial structure, can be found in real animal populations. For example, Gerum et al. (2018) observed strong regular structure in king penguin (*Aptenodytes patagonicus*) colonies, caused by short-range nest site-protecting repulsive interactions between neighbours. Gajamannage et al. (2017) studied the formation of small clusters in cows (*Bos taurus*), generated by a balancing of costs to an individual of synchronisation (e.g. needing to concede to the timings of a large group, causing interrupted rest or grazing) with the benefits of reduced predation risk for larger, more defensible groups. Olson et al. (2009) observed the formation of a mega-herd in Mongolian gazelles (*Procapra gutturosa*), driven by habitat quality in a fragmented landscape.

Some animal behaviour models also have an orientation component to make individuals move in the same direction (Sumpter et al., 2008). This is more relevant for species where individuals in a group tend to be in continuous motion, such as shoaling fish or flocking birds. These situations require a velocity jump process (Codling et al., 2007, 2008), where reorientation events depend on the distance to and current orientation of other individuals in the neighbourhood (Agueh et al., 2011). In principle, the structure of such a population could be described by a second spatial moment in terms of the difference between the positions and orientations of two individuals in a pair, but this problem is currently untackled.

Acknowledgements

RNB's PhD scholarship was funded by the Royal Society Te Apārangi Marsden fund (grant number 11-UOC-005). RNB and MJP were partly funded by Te Pūnaha Matatini. RL acknowledges funding from the University of Canterbury Erskine Fellowship scheme. We thank Alex James for discussions on an earlier version of the model and D W Franks for discussions on factors affecting group size.

References

Adams, T. P., Holland, E. P., Law, R., Plank, M. J., and Raghib, M. (2013). On the growth of locally interacting plants: differential equations for the dynamics of spatial moments. *Ecology*, 94(12):2732–2743.

Agueh, M., Illner, R., and Richardson, A. (2011). Analysis and simulations of a refined flocking and swarming model of Cucker-Smale type. *Kinetic and Related Models*, 4(1):1–16.

Barraquand, F. and Murrell, D. J. (2013). Scaling up predatorprey dynamics using spatial moment equations. *Methods in Ecology and Evolution*, 4:276–289.

Benhamou, S. (2006). Detecting an orientation component in animal paths when the preferred direction is individual-dependent. *Ecology*, 87(2):518–528.

Binny, R. N. (2016). *Spatial Moment Models for Collective Cell Behaviour.* PhD thesis, University of Canterbury, New Zealand.

Binny, R. N., Haridas, P., James, A., Law, R., Simpson, M. J., and Plank, M. J. (2016a). Spatial structure arising from neighbour-dependent bias in collective cell movement. *PeerJ*, 4:e1689.

Binny, R. N., James, A., and Plank, M. J. (2016b). Collective cell behaviour with neighbour-dependent proliferation, death and directional bias. *Bulletin of Mathematical Biology*, 78:2277–2301.

Binny, R. N., Plank, M. J., and James, A. (2015). Spatial moment dynamics for collective cell movement incorporating a neighbour-dependent directional bias. *Journal of the Royal Society Interface*, 12:20150228.

Blath, J., Etheridge, A., and Meredith, M. (2007). Coexistence in locally regulated competing populations and survival of branching annihilating random walk. *Annals of Applied Probability*, 17(5/6):1474–1507.

Bode, N. W. F. (2011). *Modelling collective motion in animals and the impact of underlying social networks*. PhD thesis, University of York, UK.

Bolker, B. and Pacala, S. W. (1997). Using moment equations to understand stochastically driven spatial pattern formation in ecological systems. *Theoretical Population Biology*, 52:179–197.

Codling, E. and Hill, N. (2005). Sampling rate effects on measurements of correlated and biased random walks. *Journal of Theoretical Biology*, 233(4):573–588.

Codling, E., Pitchford, J., and Simpson, S. (2007). Group navigation and the "many-wrongs principle" in models of animal movement. *Ecology*, 88(7):1864–1870.

Codling, E. A., Plank, M. J., and Benhamou, S. (2008). Random walk models in biology. *Journal of the Royal society interface*, 5(25):813–834.

Couzin, I. D., Krause, J., James, R., Ruxton, G. D., and Franks, N. R. (2002). Collective memory and spatial sorting in animal groups. *Journal of Theoretical Biology*, 218(1):1 – 11.

Dieckmann, U. and Law, R. (2000). Relaxation projections and the method of moments. In Dieckmann, U., Law, R., and Metz, J. A. J., editors, *The Geometry of Ecological Interactions: Simplifying Spatial Complexity*, chapter 21, pages 412–455. Cambridge University Press, Cambridge, UK.

DuVal, E. H. (2007). Adaptive advantages of cooperative courtship for subordinate male lance-tailed manakins. *The American Naturalist*, 169:423–432.

Elgar, M. A. (1989). Predator vigilance and group size in mammals and birds: A critical review of the empirical evidence. *Biological Reviews*, 64:13–33.

Gajamannage, K., Bollt, E. M., Porter, M. A., and Dawkins, M. S. (2017). Modeling the lowest-cost splitting of a herd of cows by optimizing a cost function. *Chaos: An Interdisciplinary Journal of Nonlinear Science*, 27(6):063114.

Gerum, R., Richter, S., Fabry, B., Bohec, C. L., Bonadonna, F., Nesterova, A., and Zitterbart, D. P. (2018). Structural organisation and dynamics in king penguin colonies. *Journal of Physics D: Applied Physics*, 51 164004.

Gillespie, D. T. (1977). Exact stochastic simulation of coupled chemical reactions. *The Journal of Physical Chemistry*, 81(25):2340–2361.

Griffin, R. H. and Nunn, C. L. (2012). Community structure and the spread of infectious disease in primate social networks. *Evolutionary Ecology*, 26:779–800.

Hamilton, W. D. (1971). Geometry for the selfish herd. *Journal of Theoretical Biology*, 31(2):295 – 311.

Herbert-Read, J. E., Perna, A., Mann, R. P., Schaerf, T. M., Sumpter, D. J. T., and Ward, A. J. W. (2011). Inferring the rules of interaction of shoaling fish. *Proceedings of the National Academy of Sciences*, 108(46):18726–18731.

Illian, J., Pentttinen, A., Stoyan, H., and D., S. (2008). *Statistical Analysis and Modelling of Spatial Point Patterns*. Wiley & Sons Chichester UK.

James, R., Bennett, P. J., and Krause, J. (2004). Geometry for mutualistic and selfish herds: the limited domain of danger. *Journal of Theoretical Biology*, 228:107–113.

Jeon, J., Quaranta, V., and Cummings, P. T. (2010). An off-lattice hybrid discrete-continuum model of tumor growth and invasion. *Biophysical Journal*, 98(1):37–47.

Kirkwood, J. G. (1935). Statistical mechanics of fluid mixtures. *The Journal of Chemical Physics*, 3:300–313.

Krause, J., Ruxton, G. D., and Ruxton, G. D. (2002). *Living in groups*. Oxford University Press.

Law, R., Murrell, D. J., and Dieckmann, U. (2003). Population growth in space and time: spatial logistic equations. *Ecology*, 84(1):252–262.

Lukeman, R., Li, Y.-X., and Edelstein-Keshet, L. (2010). Inferring individual rules from collective behavior. *Proceedings of the National Academy of Sciences of the United States of America*, 107:12576–80.

Maher, C. R. and Lott, D. F. (1995). Definitions of territoriality used in the study of variation in vertebrate spacing systems. *Animal Behaviour*, 49:1581–1597.

Markham, A. C., Gesquiere, L. R., Alberts, S. C., and Altmann, J. (2015). Optimal group size in a highly social mammal. *Proceedings of the National Academy of Sciences*, 112:14882–14887.

Matsiaka, O. M., Penington, C. J., Baker, R. E., and Simpson, M. J. (2017). Continuum approximations for lattice-free multi-species models of collective cell migration. *Journal of Theoretical Biology*, 422:1–11.

Middleton, A. M., Fleck, C., and Grima, R. (2014). A continuum approximation to an off-lattice individual-cell based model of cell migration and adhesion. *Journal of Theoretical Biology*, 359:220–232.

Murrell, D. J. (2005). Local spatial structure and predator-prey dynamics: counterintuitive effects of prey enrichment. *American Naturalist*, 166:354367.

Murrell, D. J., Dieckmann, U., and Law, R. (2004). On moment closures for population dynamics in continuous space. *Journal of Theoretical Biology*, 229:421–32.

Murrell, D. J. and Law, R. (2000). Beetles in fragmented woodlands: a formal framework for dynamics of movement in ecological landscapes. *Journal of Animal Ecology*, 69(3):471–483.

Murrell, D. J. and Law, R. (2003). Heteromyopia and the spatial coexistence of similar competitors. *Ecology Letter*, 6:48–59.

Olson, K. A., Mueller, T., Bolortsetseg, S., Leimgruber, P., Fagan, W. F., and Fuller, T. K. (2009). A mega-herd of more than 200,000 Mongolian gazelles Procapra gutturosa: a consequence of habitat quality. *Oryx*, 43(1):149–153.

Parrish, J. K. and Edelstein-Keshet, L. (1999). Complexity, pattern, and evolutionary trade-offs in animal aggregation. *Science*, 284(5411):99–101.

Plank, M. J. and Law, R. (2015). Spatial point processes and moment dynamics in the life sciences: a parsimonious derivation and some extensions. *Bulletin of Mathematical Biology*, 77:586–613.

Pulliam, H. R. (1973). On the advantages of flocking. *Journal of Theoretical Biology*, 38:419–422.

Raghib, M., Hill, N. A., and Dieckmann, U. (2011). A multiscale maximum entropy moment closure for locally regulated space-time point process models of population dynamics. *Journal of Mathematical Biology*, 62:605–53.

Reiczigel, J., Lang, Z., Rozsa, L., and Tóthmérész, B. (2008). Measures of sociality: two different views of group size. *Animal Behaviour*, 75:715–721.

Reluga, T. C. and Viscido, S. (2005). Simulated evolution of selfish herd behaviour. *Journal of Theoretical Biology*, 234:213225.

Sah, P., Leu, S. T., Cross, P. C., Hudson, P. J., and Bansal, S. (2017). Unraveling the disease consequences and mechanisms of modular structure in animal social networks. *Proceedings of the National Academy of Sciences of the United States of America*, 114:4165–4170.

Sumpter, D., Buhl, J., Biro, D., and Couzin, I. (2008). Information transfer in moving animal groups. *Theory in biosciences*, 127(2):177–186.

Surendran, A., Plank, M. J., and Simpson, M. (2018a). Spatial structure arising from chase-escape interactions with crowding. *bioRxiv*, page 470799.

Surendran, A., Plank, M. J., and Simpson, M. J. (2018b). Spatial moment description of birth–death–movement processes incorporating the effects of crowding and obstacles. *Bulletin of Mathematical Biology*, 80(11):2828–2855.

Wood, A. J. and Ackland, G. J. (2007). Evolving the selfish herd: emergence of distinct aggregating strategies in an individual-based model. *Proceedings. Biological sciences*, 274:1637–42.